STRESSES AND DEFORMATION OF COMPRESSED ELASTOMERIC O-RING SEALS

by
Itzhak Green and Capel English
The George W. Woodruff School of Mechanical Engineering
Georgia Institute of Technology
Atlanta, GA 30332-0405

ABSTRACT

The sealing capability of an elastomeric O-ring seal depends upon the contact stresses that develop between the O-ring and the surfaces with which it comes into contact. It has been suggested in the literature that leakage will occur when the pressure differential across the seal just exceeds the initial (or static) peak contact stress. The stresses that develop in compressed O-rings, in common cases of restrained and unrestrained geometries (grooved and ungrooved), are investigated using the finite element method. The analysis includes material hyperelasticity and axisymmetry. Contact stress profiles, and peak contact stresses are plotted versus squeeze, up to 32 percent. The contact width, which is the length of the O-ring that touches the retaining surfaces when viewed from the cross-section, is also determined. Expressions are derived empirically to predict the peak contact stress and the contact width. These expressions are also compared to those obtained by other researchers (who assumed plain strain conditions) and conclusions to their validity are drawn.

NOMENCLATURE

b	= contact width	S	= compressive stress
d	= wire diameter	x^*	= displacement
D	= nominal (mean) diameter	x	= radial coordinate
D_{def}	= deformed mean diameter	X	= radial distance from O-ring center
E	= modulus of elasticity	y	= axial coordinate
h	= deformed O-ring thickness	Y	= axial distance from O-ring center
l	= groove width	δ	= normalized squeeze (i.e., fractional compression)
q	= chord diameter		
Q	= normalized chord diameter, q/d	δ_{ij}	= equivalent normalized squeeze

83

INTRODUCTION

Elastomeric O-ring seals have a broad range of service conditions that make the O-ring ideal for static and dynamic sealing functions. Its ability to seal on relatively rough surface finishes offers one of the economical solutions to sealing problems. Elastomeric O-rings are capable of undergoing large deformations under compression. Hence, grooves are often used to restrict this deformation, resulting in improved sealing capabilities and prevention of creep and extrusion. The complex geometry confederated with the deformation of restrained O-rings and nonlinear material hyperelasticity render analytical solutions infeasible. This complicated geometry and experimental inconvenience make experimental data hard to obtain. It is here where the utility of the finite element method becomes prominent. By performing a FEM analysis, comparison of the results can be made to cases where experimental data is procurable. Then, conclusions can be drawn as to the validity of FEM solutions of geometries where experimental data cannot be easily obtained.

The stiffness relationships associated with the compression of elastomeric torroidal O-ring seals have recently been studied by Green and English (1992) for the cases shown in Figure 1. That work provided empirical expressions for the prediction of compression forces and stiffnesses at squeeze levels up to 32 percent. Sealing capabilities, however, depend upon the stress related parameters at the interface. It was as early as Lindly's work (1967), who proposed that leakage onset occurs when the pressure differential across the seal, P, barely exceeds the initial (or static) peak contact stress, S_{max} (i.e., $P \geq$

Figure 1 (A) Unrestrained Radial Loading. (B) Unrestrained Axial Loading. (C) Restrained Radial Loading. (D) Restrained Axial loading.

S_{max}). It should be noted that any increase in the contact stress, caused by the pressure loading, is ignored using this theory. Simplified expressions relating contact width to peak contact stress have been developed in order to predict S_{max}. Assuming unrestrained loading and plain strain Lindley (1967) obtained the contact width, b, normalized with respect to the wire diameter, d, [see Figures 2(a) and 3]
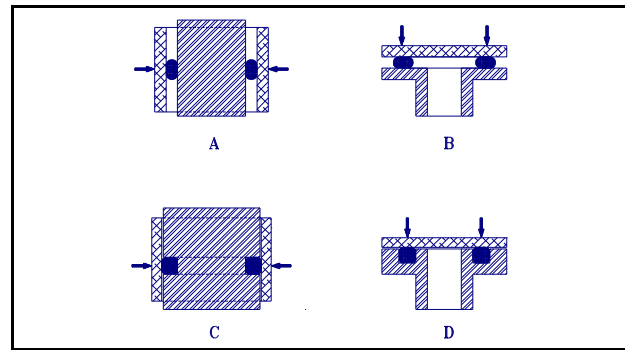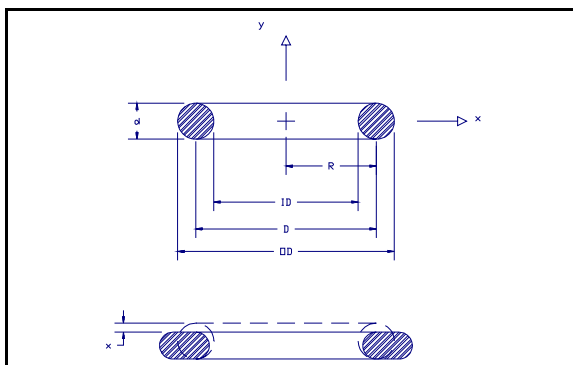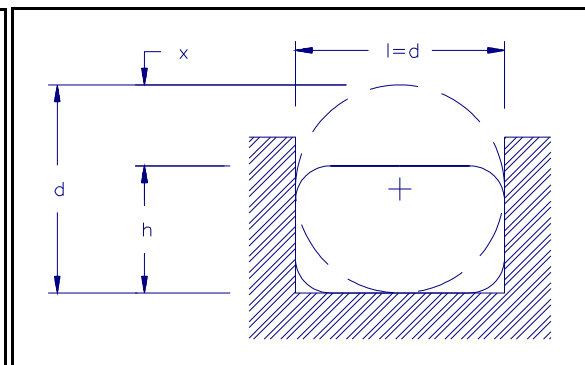

Figure 2(a) Unrestrained geometry

Figure 2(b) Section of a restrained O-ring

$$\frac{b}{d} = \left[\frac{6}{\pi} \ (1.25\delta^{\frac{3}{2}} + 50\delta^6) \right]^{\frac{1}{2}} \tag{1}$$

and the peak contact stress, S_{max}, normalized with respect to the modulus of elasticity, E,

$$\frac{S_{max}}{E} = \left[\frac{16}{6\pi} \ (1.25\delta^{\frac{3}{2}} + 50\delta^6) \right]^{\frac{1}{2}} \tag{2}$$

Here $\delta = x^*/d$, is the normalized squeeze, i.e., the compressive displacement, x^*, divided by the wire diameter, d. The first term in the equations was obtained using Hertzian theory, and the second term was added to correct for empirical data at high squeeze levels.

Wendt (1971) examined stress distributions in O-rings and X-rings, with emphasis on groove design. The most significant result of his work includes an expression for contact width of an unrestrained axially loaded O-ring. Molari (1973), who examined the stress and contact related parameters of O-rings using photoelastic techniques, lent credence to the findings of Wendt and was one of the firsts to examine the problem of restrained O-ring seals. Molari's work, however, considered one lateral wall only. Dragoni and Strozzi (1988) also used photoelasticity, but investigated an O-ring restrained between two lateral walls as defined in Figure 2(b). These researchers assumed that plane strain conditions were prevailing and thus did not address the condition of axisymmetric loading.

Figure 3 *Stress profile definition for unrestrained axial loading.*

George, Strozzi, and Rich (1987) supported Lindley's results using a finite element code developed especially for the task. Experimental data taken was compared to the results obtained by numerical solution. Later Dragoni and Strozzi (1988) examined the case of laterally restrained O-ring seals in a groove using a modification of the FEM code. The results were also limited to plain strain conditions. Using Lindley's model of Hertzian contact stress, they offered an approximate analytical method for "moderately" compressed O-rings up to about 15 percent squeeze. A stress related parameter was given in terms of a normalized deformed chord diameter, $Q = q/d$ (see Figure 3). By fitting a curve to experimental results (Strozzi, 1986), they characterized Q as a function of δ

$$Q = 1 + 0.415 \ \delta + 1.15 \ \delta^2 \equiv f(\delta) \tag{3}$$

where the right-hand side emphasizes the functional form of the equation, as needed for later derivations. Using only the first term of Eq. (2) the peak contact stress was given as

$$\frac{S_{max}}{E} = \sqrt{\frac{10}{3\pi}} \ \delta^{\frac{3}{4}} \tag{4}$$

In a compromise between accuracy and simplicity they prefer Wendt's (1971) description of the contact width
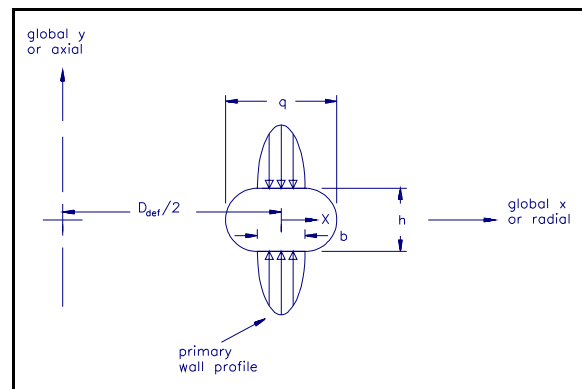
$$\frac{b}{d} = \frac{3}{2} \delta^{\frac{2}{3}}$$

(5)

At this point Dragoni and Strozzi (1988) developed an equivalent normalized squeeze, δ_{ij}, which can be used in modeling the characteristics of restrained O-rings. The notation ij is used to denote the effects of the particular groove wall defined perpendicular to either the i or j direction. For example, for restrained radial loading the equivalent squeeze in the x direction, δ_{xy}, denotes the squeeze associated in part to the squeeze directly applied in the x direction and in part to the constraint of the walls which are perpendicular to the y direction. Alternately, for restrained axial loading, δ_{yx} is the equivalent normalized squeeze on the groove walls perpendicular to the top/bottom compressive surfaces. By definition δ_{yx} is estimated as a ratio. The numerator is the difference between two terms: (i) a virtual deformed chord diameter along the y-axis caused by the compression δ_{xy} [and is calculated by substituting δ_{xy} into Eq. (3)]; (ii) the deformed O-ring thickness, h [shown in Figure 2(b)]. The denominator is the undeformed wire diameter, d. Hence,

$$\delta_{yx} = \frac{d \cdot f(\delta_{xy}) - h}{d} = f(\delta_{xy}) - \frac{h}{d}$$

(6)

where f is the functional given in Eq. (3). Applying similar reasoning in the perpendicular x-direction, and using the groove width, l (as the O-ring thickness), gives the equivalent squeeze

$$\delta_{xy} = \frac{d \cdot f(\delta_{yx}) - l}{d} = f(\delta_{yx}) - \frac{l}{d}$$

(7)

These relationships provide estimates for any groove dimensions (allowing the possibility of a gap between the undeformed O-ring and the lateral walls, i.e., $l > d$). Next, we define the particular case (subscripted here with the letter t) where the groove lateral walls are tangent to the undeformed O-ring, i.e., $l = d$ as shown in Figure 2(b). Combination of Eqs. (6) and (7) yields

$$\delta_{tyx} = f(f(\delta_{tyx}) - 1) - \frac{h}{d}$$

(8)

where the functional form of Eq. (3) is used repeatedly. Eq. (8) can be solved iteratively for δ_{tyx}. Then δ_{txy} is calculated by Eq. (7), and by substitution into Eqs. (4) and (5) the normalized peak contact stress and the normalized contact width can be determined in the respective directions.

Since in all the aforementioned work plain strain conditions prevailed, it implies that no distinction exists between axial and radial loading. This was found invalid in some important loading conditions for the compression force and stiffness (Green and English, 1992). The loading cases in Figure 1 are investigated here to determine contact stresses and contact widths under axisymmetric conditions. These include a highly frictional ("unlubricated") contact where surface sliding is prevented in an unrestrained axial loading; and frictionless ("perfectly lubricated") contacts where forceless surface sliding exist in axial, radial, restrained, and unrestrained loadings. The commercial code ANSYS and the nonlinear techniques, described in Green and English (1992) and in greater detail in English (1989), are utilized. Reduced integration is exclusively applied as it was found to give most accurate results. These are best represented in normalized forms, proven indifferently to the aspect ratio, d/D. Convergence is discussed in whole in the last two references.

STRESS PARAMETERS RESULTS

Vernacular for this discussion includes "primary wall" and "lateral wall." The primary wall or walls are the surfaces which move together to force the compression of the O-ring. The lateral walls are the sides of the restraining groove. Initially all walls are tangent to the undeformed geometry of the O-ring. For the axial case the top and bottom walls are the primary walls, and for the radial case the inside and outside walls are the primary walls.

Contact stress profiles are plotted as the normalized nodal stress component, S_y/E or S_x/E, versus the normalized x or y coordinates (X/d or Y/d), respectively. For example, Figure 3 shows the X-coordinate, defined relative to the deformed nominal radius, $D_{def}/2$. X is the horizontal distance from the center of the O-ring cross-section to a node along the perimeter. The normalized stress of interest here is the y-component of the nodal stress, S_y/E. In the plots E_o is shown instead to designate neo-Hookean material representation, justified for use by Green and English (1992).

The first contact pressure profile, shown in Figure 4, was produced from a quadrilateral element mesh, using reduced integration (Green and English, 1992). Six profiles were chosen
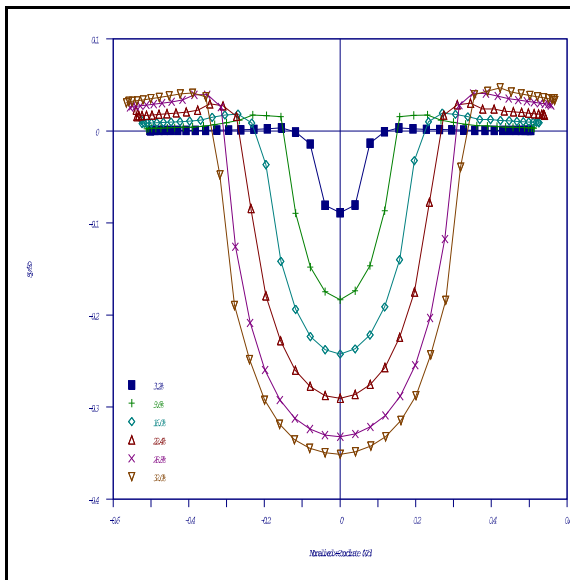

Figure 4 *Primary wall contact stress profile for unrestrained - perfectly lubricated axially loaded O-ring.*
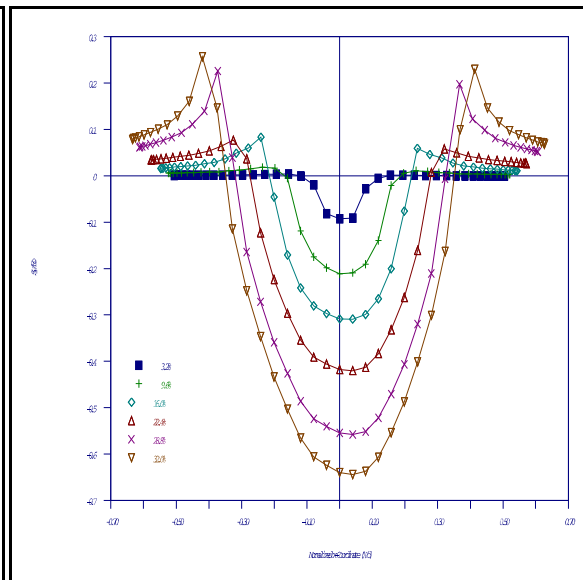
Figure 5 *Primary wall contact stress profile for unrestrained - unlubricated axially loaded O-ring (the only fixed case)*

from ten load steps of 3.2 percent squeeze each, and are represented by the symbols given in the legend. Two other features can be extracted from the figure: (i) The normalized deformed chord diameter, Q=q/d, is the farthest distance between two opposite points on each profile, and (ii) the normalized contact width, b/d, is the distance between two points on each profile where the curve intersects the zero stress line. Notice that Q and b/d are different at each load step. Finally, there is a condition of symmetry about the x-z plane, of the global coordinate system, such that both the top and bottom profiles are identical and, therefore, only one is shown. While the profiles appear symmetric about X/d=0, close examination of the results reveals otherwise. This is due to the imposition of axisymmetric conditions upon the solution (rather than plain strain conditions).

Figure 5 shows the contact stress profile for the unlubricated case of unrestrained axial loading (where a coefficient of friction 0.9 was used). The asymmetry is much more pronounced in

this case. It should also be noted that the peak value of S_y is roughly 85 percent higher than that for the lubricated case. This increase in peak contact stress can be explained by the fact that the deformed nominal diameter, D_{def}, does not expand as the load increases. Actually D_{def} decreases as the loading is applied, although, only a small amount. A comparison of Figures 4 and 5, shows that friction has a dominating role in stress profile development.

Turning to radial compression, Figure 6 shows how the contact stress profiles are defined. S_x is the stress component of interest here, and Y is the vertical distance from the center of the
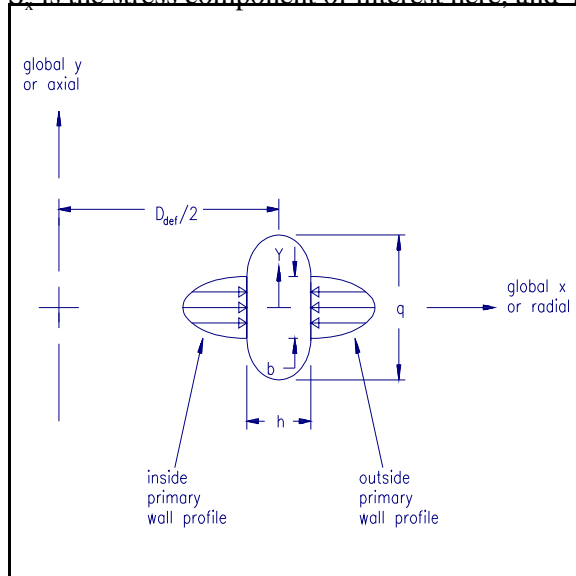

Figure 6 *Stress profile definition for unrestrained radial loading.*
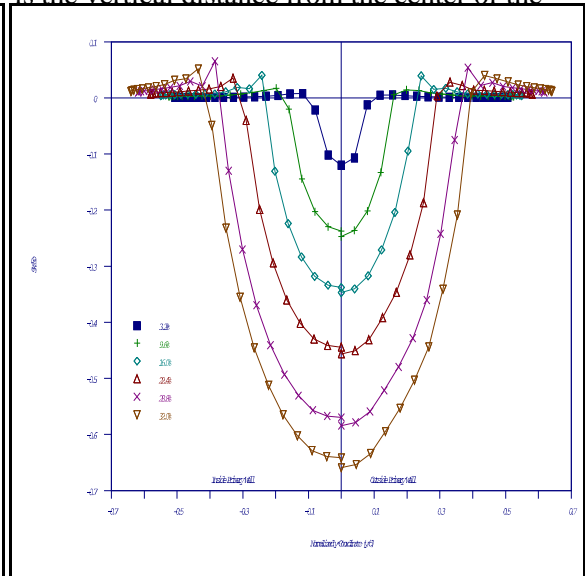

Figure 7 *Contact stress profile for unrestrained radial loading. Half profiles for the inside and outside primary walls are shown.*

O-ring cross section to a node on the perimeter. q is the deformed chord diameter parallel to the compressive surfaces. Because the model is not symmetric about the y-z plane the stresses on both walls, the inside primary wall and the outside primary wall, must be examined.

The stress profiles for unrestrained radial loading are shown in Figure 7. Here we notice that the outside primary wall profile is larger than the inside primary wall profile. This is due to nominal diameter contraction during axisymmetric loading. Figure 7 exemplifies again the necessity of using an axisymmetric model to represent the O-ring. While the difference between the inside and outside walls is minor for this particular restraining configuration it could be much more significant for a different type of loading.

Next up for attention are the restrained cases. Figure 8 gives the profile definition for restrained axial loading. Note that the profiles are symmetric about the x-z plane; however, they
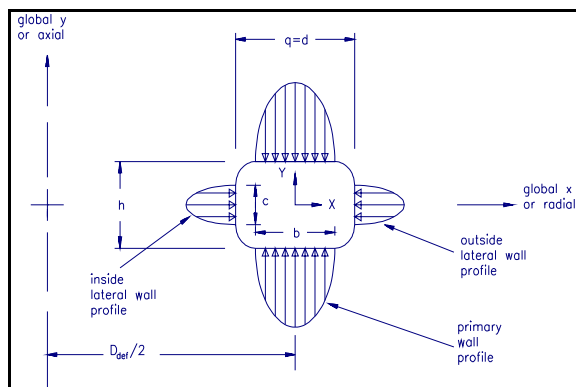

Figure 8 *Profile definition for restrained axial loading.*
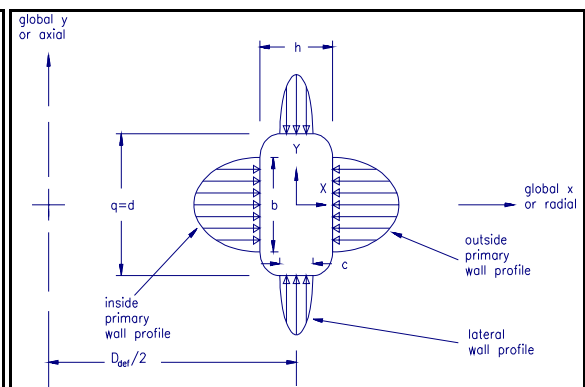

Figure 9 *Profile definition for restrained radial loading.*

are not symmetric about the y-z plane. The restrained radial profile definition can be seen in Figure 9. This profile is similar to the previous profile in that the symmetry planes are the same. However, the primary and lateral walls are different. Note the definitions for the contact widths *b* and *c* on the primary and lateral walls, respectively.

Figures 10 and 11 show the profiles for the primary and lateral walls, respectively, for the restrained axially loaded O-ring. The half profiles for the inside and outside lateral walls show
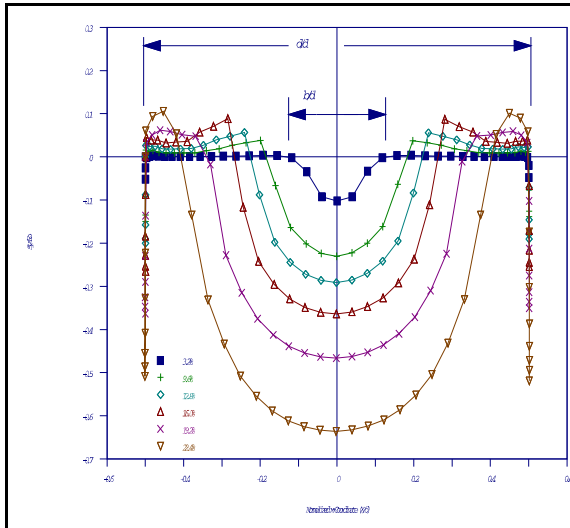

Figure 10   Contact stress profile for primary wall of restrained axial loading.
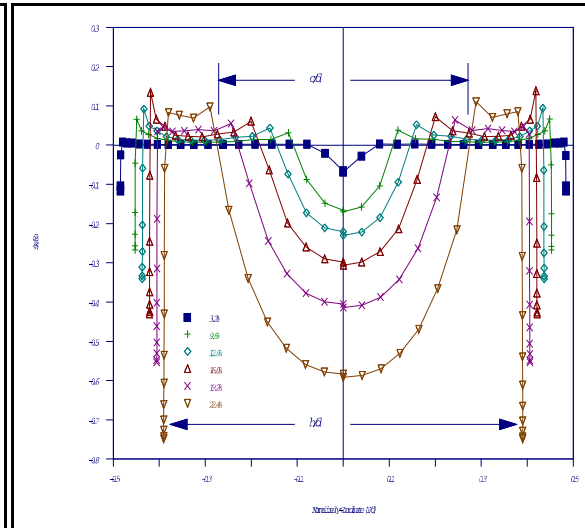

Figure 11   Contact stress profile for inside and outside lateral walls for restrained axial loading.

that there is a difference between lateral wall profiles where axisymmetric loading is concerned. Here the peak value of S/E_o is 17 percent larger for the primary wall than that for the lateral wall. Figures 10 and 11 show an interesting formation of significant compressive normal stresses at the O-ring surface that is in contact with the respective retaining walls. Molari (1973), using bidimensional photoelastic techniques, obtained similar profiles; however, the surface stresses did not show up in his work because they were masked by the physical boundary of the test apparatus.
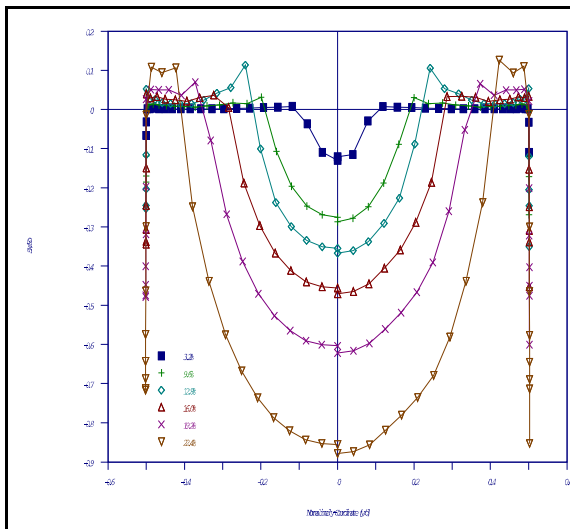

Figure 12   Contact stress profile for inside and outside primary walls for restrained radial loading.
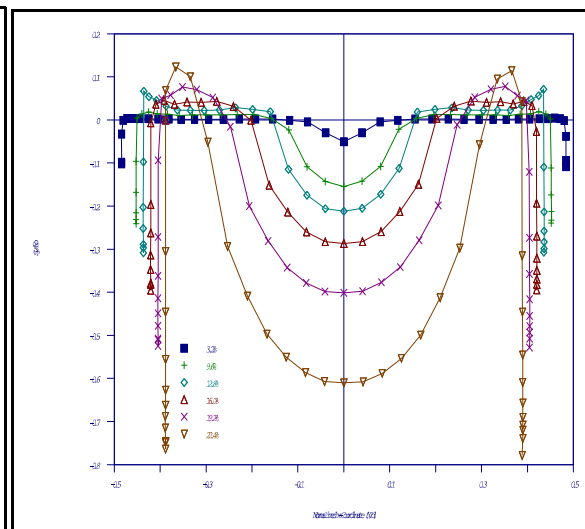

Figure 13   Contact stress profile for lateral wall of restrained radial loading.

Next we consider the case of restrained radial loading. Contact stress profiles for the primary and lateral walls are given in Figures 12 and 13, respectively. In Figure 12 a difference exists in the half profiles for the inside (left) and outside (right) primary walls. Peak contact stress values for the primary walls are about 34 percent greater than those for the lateral wall. Also here there are surface stresses at the retaining walls.

The final case under investigation is that for plane strain loading. Figure 14 shows the stress profile for unrestrained plane strain loading. Plane strain loading profiles for the restrained case are given in Figures 15 and 16. In this case there is symmetry about both the x-z and y-z planes. Hence, there is no need for a half profile plot of inside or outside walls. It can be seen by comparing the stress profiles

Figure 14   *Contact stress profile for unrestrained plane strain loading primary wall.*

from plain strain loading to all previous cases that there is a significant difference in the profiles, especially in radial loading and peak contact stresses. It is, therefore, concluded that plain strain conditions do not commonly describe O-ring compression.
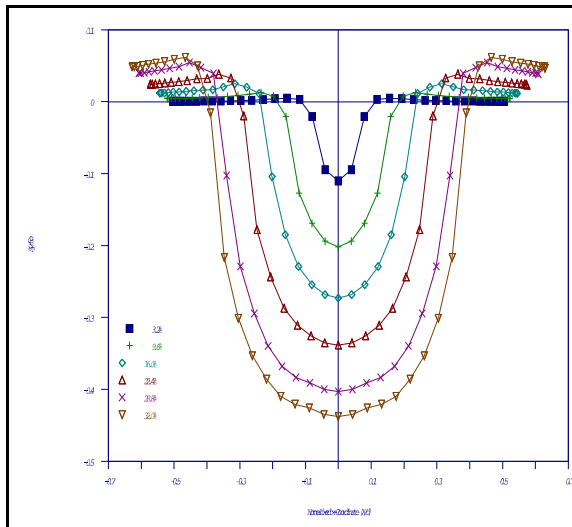

Figure 15   *Contact stress profile for restrained plane strain loading primary wall.*
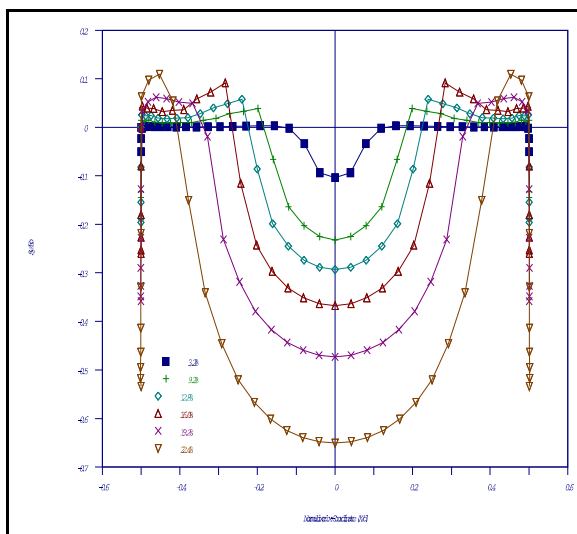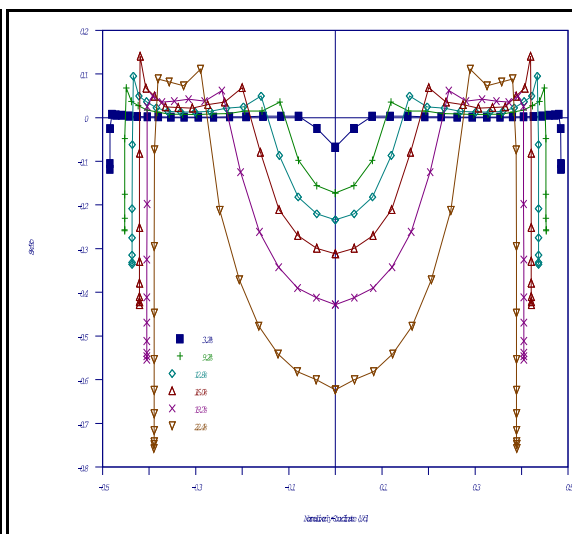

Figure 16   *Contact stress profile for plane strain loading lateral walls.*

PEAK CONTACT STRESS

Peak contact stress is of interest in order to estimate the ability of the O-ring to form a seal (Lindley, 1967). Figure 17 contains the compilation of peak contact stresses for unrestrained loadings, i.e., axial, radial, and plane strain. It can be seen that the primary wall peak contact stress response for radial loading is the greatest. This is followed by the stress response of the unlubricated axial loading, which is significantly greater than its lubricated correlative. Furthermore, we see that both Lindley's predictions underestimate the peak contact stress throughout the loading range with the exception of the plane strain case. The latter case agrees relatively well with the prediction Lindley derived from Hertzian theory (Eq. (2), but without the second correction term). Note that

the empirically added correction term causes an overestimation of the peak contact stress for squeezes above 24 percent.

Lindley gives no prediction for the peak contact stress of a restrained O-ring. The comparison to Dragoni and Strozzi (1988) prediction can be seen in Figures 18 and 19. Their prediction agrees relatively well with the axial and plane strain results, but, underestimates the peak contact stress for radial loading. Where the lateral wall is concerned Strozzi's prediction underestimates the peak contact stress response for all cases. It is interesting that the lateral wall response for radial loading is less than the responses for both axial and plane strain cases. It seems from this comparison, that Strozzi's model is relatively accurate for predicting the peak contact

Figure 17 *Peak contact stress results for unrestrained loading.*

stress for the primary wall of restrained axial and restrained plane strain cases, but it breaks down in radial loading and where the lateral wall is concerned.
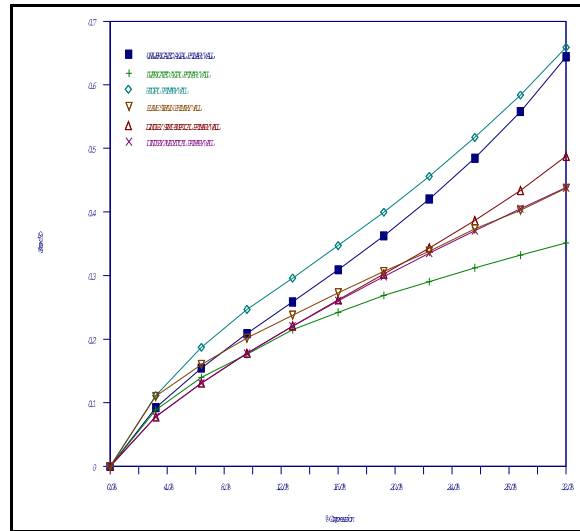

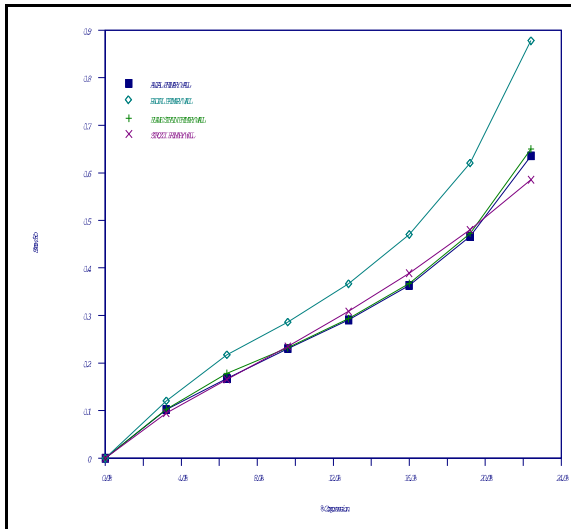**Figure 18** *Peak contact stress results for restrained loading primary wall.*
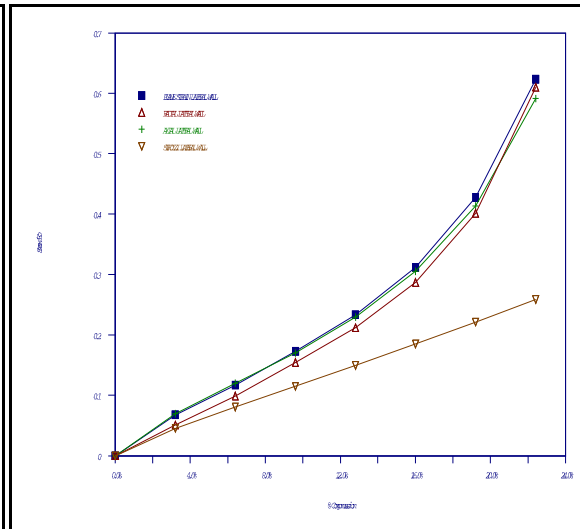
Figure 19 *Peak contact stress for restrained loading lateral wall.*

The lack of agreement to analytical work prompts the determination of the peak contact stress from the numerical data. This is accomplished by fitting a polynomial to the numerical results. Second and third order polynomials are proposed as follows:

$$\frac{S_{\max}}{E} = a\delta + b\delta^2 \tag{9}$$

$$\frac{S_{\max}}{E} = c\delta + d\delta^2 + e\delta^3 \tag{10}$$

where the coefficients are given in Table 1. While Eq. (10) produces an excellent fit, Eq. (9) may be used for simplicity with satisfactory results.

Table I *Least squares coefficients for the calculation of the peak contact stress*

Loading Case	a	b	c	d	e
Unrestrained lubricated axial primary wall	2.0572	-3.1417	2.6296	-8.8589	12.8391
Unrestrained unlubricated axial primary wall	2.0090	-0.2211	2.8383	-8.5051	18.6031
Unrestrained lubricated radial primary wall	2.4891	-1.5967	3.4591	-11.2857	21.7583
Unrestrained lubricated plane strain primary wall	2.2340	-2.8961	3.0373	-10.9192	18.0171
Restrained axial primary wall	1.9715	3.1502	3.8295	-23.0013	82.6963
Restrained axial lateral wall	1.0497	6.4631	2.6584	-16.1793	71.5999
Restrained radial primary wall	2.1587	6.7729	4.9363	-32.3232	123.630
Restrained radial lateral wall	0.5844	8.7930	2.3003	-15.3593	76.3744
Restrained plane strain primary wall	1.9933	3.2711	4.0499	-25.6765	91.5384
Restrained plane strain lateral wall	0.9400	7.5182	2.6698	-16.8290	76.9908

CONTACT WIDTH RESULTS

In Figure 3 the contact width, b, is defined as the length of the circumference of the O-ring, from a cross-sectional view, that makes contact with the compressing surface. This information is useful in calculating the total load required to compress the O-ring and in determining the contact stress profile when using Hertzian theory. Both Lindley (1967) and Wendt (1971) propose expressions which approximate the contact width as a function of compression for unrestrained loading, and Dragoni and Strozzi (1988) propose corresponding expressions for restrained loading. As illuminated in the introduction these were developed assuming plain strain conditions. This section compares results obtained in this research to those predicted by the other researchers.

Figure 20 *Normalized contact width as a function of compression for unrestrained loading. Included are Lindley and Wendt's prediction as well as the results from nodal displacements.*

The error associated with the numerical results is significant when considering the technique used to obtain the contact width. In Figure 20 there are several data points with approximately identical values of b/d. This comes from the discrete points used to obtain the contact width. As the loading is applied, new nodes may or may not come into contact with the compressing surfaces. Several data points with the same value of b/d imply that no new nodes have come into contact during that portion of the loading sequence. Physically the contact width response is a continuous phenomenon. By discretizing the mesh we turn this response into a discrete phenomenon. Consequently the first data point, of those which have the same magnitude of b/d, is
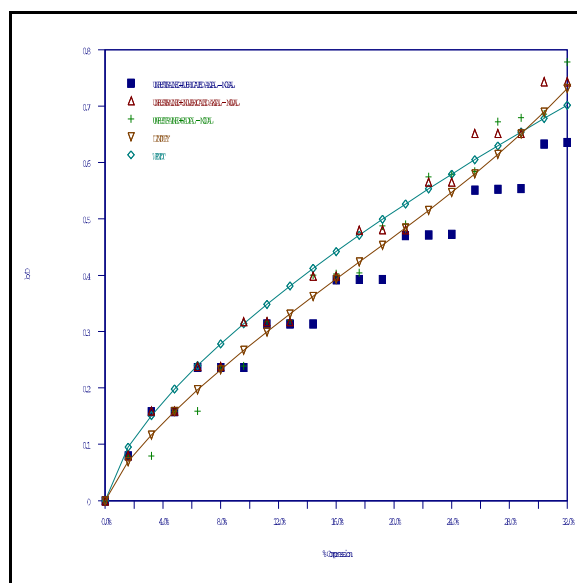
the most accurate. Therefore, the contact width shown is an underestimation of the actual contact width.

Contact width data, for the cases of unrestrained loading can be seen in Figure 20. The numerical results from the unlubricated axial and radial cases agree well with Wendt's prediction, Eq. (5), up to roughly 24 percent compression. Lindley's prediction, Eq. (1), underestimates the numerical contact width throughout the load range. For the lubricated axial load case Wendt's expression begins to overestimate the contact width at approximately 10 percent compression while Lindley's expression underestimates, at low compression, and over estimates it at higher compressions. From this we may conclude that Wendt's prediction is good for small compressions and that Lindley's prediction should generally not be used.

Now we turn to restrained loading while probing Strozzi's approach as outlined from Eq. (3) through Eq. (8). To do so a second order polynomial [similar to Eq. (3)] must first be fitted to the data obtained from the FE analysis of the three unrestrained loading results (lubricated and unlubricated axial loading, and radial loading). By extracting nodal displacements from the output it is possible to obtain the normalized deformed chord diameter. For the unlubricated-unrestrained axial loading case the fitted polynomial is

$$Q = 1 + 0.210\delta + 0.657\delta^2 \tag{11}$$

For the lubricated-unrestrained axial loading case the polynomial obtained is

$$Q = 1 + 0.361\delta + 1.547\delta^2 \tag{12}$$

and for the unrestrained radial loading case the polynomial obtained is

$$Q = 1 + 0.355\delta + 1.626\delta^2 \tag{13}$$

The contact width results for restrained loading can be examined in Figures 21 and 22 for the primary wall and lateral walls, respectively. Looking at Figure 21 we see that the predictions
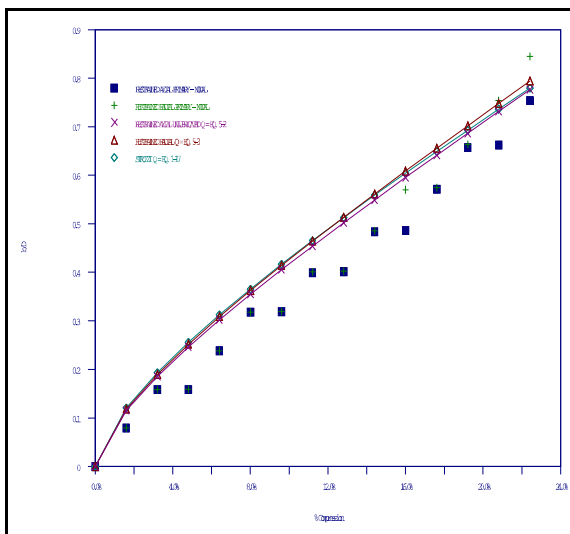

Figure 21 *Contact width as a function of compression for the primary wall of a restrained O-ring.*
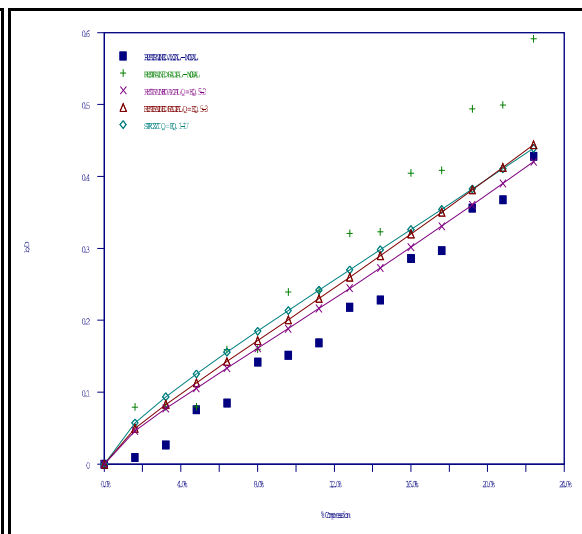

Figure 22 *Contact width as a function of compression for the lateral wall of a restrained O-ring.*

in the solid lines, using Eqs. (12) and (13) as well as Strozzi's Eq. (3), produce overestimates compared to the numerical nodal contact width at the primary wall for compressions below 19 percent. At the extreme compressions the normalized chord diameter technique underestimates the contact width of the primary wall of a restrained radially loaded O-ring. However, as mentioned above, these numerical data points underestimate the actual contact width. Therefore, the prediction may be considered to give a fairly accurate prediction of contact width.

In Figure 22 we see that Strozzi's technique is a closer approximation to the lateral wall contact width of a restrained axially loaded O-ring. But, the figure also shows that the technique is a gross underestimate of the lateral wall contact width for a restrained radially loaded O-ring. Without more experimental results it is hard to make a firm statement as to the accuracy of either Strozzi's approach or the current numerical approach. It can generally be said, however, that the numerical results underestimate the actual contact width and, therefore, the method Strozzi suggests is valid, with exception to the radially loaded case at the lateral wall.

CONCLUSIONS

Acquisition of the stress parameters requires more effort in the postprocessing phase of a finite element analysis, but compared to the extensive testing equipment required for experimental stress data acquisition, this methodology is far less expensive in terms of resources and time. Another feature that FEA has to offer is the ability to examine surface stress data that is otherwise hidden by the boundary of experimental apparatus.

The most profound finding of this work is the identification of a significant difference between the peak contact stress response of plane strain models and axisymmetric models of hyperelastic O-rings (see Figs. 17 through 19, and Table 1). This is particularly true for the case of unrestrained loading . The plane strain results obtained agreed well with those predicted by Wendt. However, Wendt's prediction of peak contact stress response greatly underestimated the response generated by axisymmetric loading. Results obtained from axisymmetric modeling of the lubricated-axially loaded O-ring also indicate that the plane strain assumption is not valid for prediction of the peak contact stress response for this particular case.

Contact width examinations performed in this work yield the most inconclusive results out of all the topics investigated. This is primarily because the mesh is finite at the perimeter and only discrete information about the contact width is available. Clearly better results can be obtained with a much refined mesh at the expense of computer time. Given the results for unlubricated-unrestrained axial loading reasonable agreement exists with Wendt's prediction for compressions up to 15 percent. Lindley's prediction underestimates the contact width response for all cases except lubricated-unrestrained axial loading.

Looking at the cases of restrained loading, only Strozzi offered an analytical technique of predicting contact width and stress. To conform with that technique the numerical results were fitted to produce expressions for the normalized chord diameter in Eqs. (11) - (13). However, the use of these equations, in the procedure outlined from Eq. (3) through Eq. (8), overestimates the contact width compared to numerical data obtained from the deformed nodal coordinates. Strozzi's prediction underestimates the lateral wall stress response for the axisymmetric axial and plane strain cases, yet it gives relatively good agreement to the axisymmetric radial case for compressions below 10 percent. For compressions above 10 percent Strozzi's prediction again underestimates the peak contact stress response.

Due to the lack of consistent agreement between the results obtained here and previous analytical work an alternate empirical procedure is proposed. The peak contact stresses can be determined using Eqs. (9) or (10) for the ten loading conditions listed in Table 1. According to Lindley (1967) these equations provide estimates of the maximum pressure an O-ring can seal.

ACKNOWLEDGMENT

REFERENCES

Dragoni, E., and Strozzi, A., 1988, "Analysis of an Unpressurized Laterally Restrained, Elastomeric O-ring," Trans. ASME, Journal of Tribology. Vol. 110, No. 2, pp. 193-199.

English, C., 1989, "Stiffness Determination of Elastomeric O-Rings Using the Finite Element Method," M.S. Thesis, Georgia Institute of Technology.

George, A.F., Strozzi, A., and Rich, J.I., 1987, "Stress Fields in Compressed Unconstrained Elastomeric O-ring seals and a Comparison with Computer Predictions with Experimental Results," Tribology International Vol. 20, pp.237-247.

Green, I., and English, C., 1992, "Analysis of Elastomeric O-ring Seals in Compression Using the Finite Element Method," STLE Trib. Trans., Vol. 35, No. 1, pp. 83-88.

Lindley, P.B., 1967, "Compression Characteristics of Laterally Unrestrained Rubber O-ring," J. IRI, Vol. 1, pp. 202-213.

Molari, P.G., 1973, "Stresses in O-ring Gaskets," 6th Int. Conf. on Fluid Sealing BHRA, pp. B2/15-31.

Strozzi, A., 1986, "Experimental Stress-Strain Field in Elastomeric O-ring seals," Experimental Stress Analysis (H. Wieringa ed.), Martinus Nijhoff Publ., pp. 613-622.

Wendt, G., 1971, "Investigation of Rubber O-ring and X-rings, 1. Stress Distributions, Service and Groove Design," BHRA Fluid Engineering, Internal Report T1115.